Nanoscale

Controlled Porous Structures of Graphene Aerogels and Their Effect on Supercapacitor Performance

Journal:	*Nanoscale*
Manuscript ID:	NR-COM-12-2014-007564.R1
Article Type:	Communication
Date Submitted by the Author:	28-Jan-2015

Complete List of Authors:	Jung, Sung Mi; Massachusetts Institute of Technology, Electrical Engineering and Computer Sciences Mafra, Daniela; Massachusetts Institute of Technology, Electrical Engineering and Computer Sciences Lin, Cheng-Te; Massachusetts Institute of Technology, Electrical Engineering and Computer Sciences Jung, Hyun Young; Northeastern University, Mechanical and Industrial Engineering Kong, Jing; MIT, Department of Electrical Engineering and Computer Science

Controlled Porous Structures of Graphene Aerogels and Their Effect on Supercapacitor Performance

Sung Mi Jung, Daniela Lopes Mafra, Cheng-Te Lin, Hyun Young Jung, and Jing Kong**

Dr. S. M. Jung, Dr. D. L. Mafra, Prof. J. Kong
Department of Electrical Engineering and Computer Sciences, Massachusetts Institute of Technology, 77 Massachusetts Avenue, Cambridge, MA 02139, USA
E-mail: jingkong@mit.edu
Dr. C-T Lin,
Department of Mechanical Engineering, Massachusetts Institute of Technology,
77 Massachusetts Avenue, Cambridge, MA, 02139, USA
Dr. H. Y. Jung
Department of Mechanical and Industrial Engineering, Northeastern University,
360 Huntington Avenue, Boston, MA 02115, USA
E-mail: hjung@coe.neu.edu

The design and optimization of 3D graphene nanostructures are critically important since the properties of electrochemical energy storages such as supercapacitor can be dramatically enhanced by tunable porous channels. In this work, we develop porous graphene aerogels from graphene suspensions obtained via electrochemical exfoliation and explore their application as supercapacitor electrodes. By adjusting the content of the electrolyte in the exfoliation process, the aspect ratio of graphene sheets and the porosity of the graphene network can be optimized. Furthermore, the freezing temperature in the freeze drying step is also found to play a critical role in the resulting pore size distributions of the porous networks. The optimized conditions lead to meso- and macro-porous graphene aerogels with high specific surface area, extremely low densities and superior electrical properties. As a result, the graphene aerogel supercapacitors exhibit a specific capacitance of 325 $F\,g^{-1}$ at 1 $A\,g^{-1}$ and an energy density of 45 $Wh\ kg^{-1}$ in 0.5 M H_2SO_4 aqueous electrolyte with high electrochemical stability and electrode uniformity required for the practical usage. This research provides a practical method for lightweight, high-performance and low-cost materials in the effective use of energy storage systems.

Porous graphene materials have attracted vast interests due to their large theoretical surface area (2600 $m^2 g^{-1}$), unique porous structures, and excellent electrical conductivity.[1-4] These extraordinary features enable porous graphene materials to serve as key components in high-performance supercapacitors with their highly open porous structure allowing electrolytes access to the surface of porous frameworks.[5-7] Most porous graphene materials are derived from graphene oxide (GO) or reduced GO (rGO),[8-15] however in many cases pristine graphene structures are more desirable.

We have previously produced the porous graphene aerogel from pristine graphene suspension obtained by using surfactant and sonication assisted solution exfoliation.[16] Graphite flakes were first exfoliated with surfactant in DI water using ultra-sonication at a dilute concentration, and then the suspension was transformed into a graphene gel by evaporating the solvent to reach the gel formation concentration ($\varphi_{gel} = a_r^{-1}$, where a_r is the aspect ratio of graphene nanosheet: $a_r=L/t$, and L is the lateral size and t is the thickness).[16] Nevertheless, for this method, the yield of graphene nanosheet are limited, making it difficult for large scale production of the porous networks. Furthermore, extensive sonication tends to result in graphene sheets with very small lateral size (hundreds nanometers) and lower aspect ratio, which would require higher gel formation concentration to form a gel, as a result, the porous networks' properties (high density, low porosity, etc) and performances in applications become limited.

During the past several years, electrochemical exfoliation of graphite has also been developed which allows the simple and large scale production of graphene sheets with more pristine qualities than rGO.[8-15] These graphene sheets are produced in aqueous solution at relatively high concentrations without the use of surfactants, with large lateral sizes (several micrometers) and thin thickness (~few layers), which greatly facilitate the formation of 3D graphene network structures of hydrogels and aerogels.

In this work, we produced highly conductive and porous graphene aerogels from graphene suspension obtained by using the electrochemical exfoliation and explored the applications of these aerogels as electrodes for supercapacitors. We have found that the pore structure of graphene aerogels can be designed and optimized by tuning the aspect ratio of graphene sheets through adjustment of the exfoliation condition. Furthermore, the freeze drying temperature is also found to play a critical role in the resulting pore size distribution of the graphene structure. The optimized graphene aerogels have very low density, higher porosity and surface area, with pore sizes ranging from several nanometers to several tens of micrometers, and remarkable electrical conductivity. The process here is very simple and allows large-scale production at a low cost. The study of supercapacitors using these electrodes have shown that such highly controlled meso- and macroporous structures of the graphene aerogels allow multidimensional electron transport and rapid electrolyte ions diffusion, which greatly enhanced the supercapacitor performances. Furthermore, electrodes made by this method demonstrate extraordinary structural stability and uniformity, which allows the construction of several supercapacitors in series and in parallel for practical usages.

We used the electrochemical exfoliation method to obtain high quality and large area thin graphene sheet suspensions for the formation of hydrogels and aerogels. Sulfuric acid (H_2SO_4) and potassium hydroxide (KOH) were used as electrolyte. The high concentration of H_2SO_4 solution affect exfoliation of graphites into much thinner graphene sheets, because the SO_4^{2-} is working as intercalator in sulfuric acid, while the high acidity play a major role to make defect on the graphene sheets. Therefore, KOH was added to reduce graphene oxidation by the acidic electrolyte (0.2 M H_2SO_4).[17-18] Alternating currents of ±1 A at 0.2 Hz were applied between the two graphite electrodes (Fig. S1a†). By using graphite as both electrodes (as in contrast to graphite only as the anode previously), the exfoliation occurs at both

electrodes resulting in higher exfoliation efficiency. The color change of the aqueous electrolyte solution from transparent to dark was observed after only a few minutes, indicating a high exfoliation rate and very efficient process. These exfoliated graphene sheets were washed with DI water and then uniformly dispersed in ethanol without using any surfactant (Fig. S1b†). The resulting graphene suspension appears very homogeneous likely due to the presence of the functional groups on the graphene sheets and the remaining ions (such as SO_4^{2-}) in the suspension.[17]

The graphene gel was formed from interlinking of the graphene sheets by concentrating the uniformly dispersed graphene suspension up to gel formation concentration (ϕ_{gel}). Here the gel formation concentration is lower than ϕ_{gel} made from sonication exfoliation[16] because the electrochemical exfoliation provides thinner and larger-area graphene sheets. Afterwards the gels were frozen at different freezing temperatures, and were transformed into graphene aerogels via the sublimation of the frozen solvent (ice) directly into water vapor. In order to obtain graphene sheets with a much higher aspect ratio (i.e., thinner in thickness and larger in area) so that aerogels with lower densities and better pore structures can be achieved, we tuned the aspect ratio by adding various amount of KOH into the H_2SO_4 electrolyte (volume ratio of the original H_2SO_4 electrolyte: KOH solution = 9:1, with KOH having different concentrations: 23, 30, and 37 wt%)(Fig. 1a). It was observed that lower concentration of KOH results in thinner but smaller exfoliated graphene sheet (Fig. S2†). The optimum aspect ratio is achieved with 30 wt% KOH (Fig. 1e), where large-area thin graphene sheets with 3.7±1 μm of the lateral size (Fig. 1b) and 2.5±0.1 nm of thickness (Fig. 1c and Fig. S1c†) were obtained. Fig. 1d and e compares the graphene aerogels made from graphene sheets having two different aspect ratios (aspect ratio of 958 from 23% KOH and aspect ratio of 1480 from 30% KOH; the rest processing conditions (such as freeze drying) are all the same). By comparing Fig. 1d and 1e, it can be seen that the aerogel made with larger aspect ratio

graphene sheets have larger pore sizes. Furthermore, the graphene aerogel derived from the sheets made with 30% KOH has a density of 6.5 mg cm^{-3}, lower than the one made with 23% KOH (11.5 mg cm^{-3}). As a result, for the later part of the investigation, we focus on the aerogels made with graphene sheets produced by 30% KOH, which are ultralight, flexible and bendable (Fig. 1f). Fig. 1g shows the electrical measurement result of the graphene aerogel in Fig. 1e, an electrical conductivity of 509 S m^{-1} was obtained. Considering the density of this aerogel is only 6.5 mg cm^{-3}, this number is remarkable. As a comparison, a conductivity of 273 S m^{-1} with two times higher density (13 mg cm^{-3})[16] was obtained in our previous graphene aerogel using sonication exfoliated graphene, and a conductivity of 100 S m^{-1} with five times higher density (10 mg cm^{-3})[11] was obtained in graphene aerogel made by reduced graphene oxide. Such extraordinary electrical characteristic suggests the high quality nature of not only the graphene network, but also the sheets obtained from the electrochemical exfoliation.

We have also found that the freeze drying temperature play a critical role in the resulting porous morphology of the graphene aerogels, similar to the recent finding by X. Xie et.al.[8] The Scanning electron microscopy (SEM) images in Fig. 2a-c show morphology of graphene aerogels made at different freezing temperatures (-200 °C (Fig. 2a), -80 °C (Fig. 2b), and -20 °C (Fig. 2c)). These images reveal clearly that the freeze-dried graphene aerogels have an interconnected 3D macro-porous network with pore sizes in the range of sub-micrometers to several tens of micrometers. By comparing among them, it shows that even though the same graphene gels were used before the freeze drying, different freezing temperatures give rise to different morphologies of the graphene network. The macro-pore size increases as the freezing temperature increases and especially enlarges up to 60 μm at high freezing temperature of -20 °C. Since the graphene gels were directly brought from room temperature to these freezing temperatures, different freezing temperature will imply different freezing (or

ice solidifying) rate. At a low freezing temperature of -200 °C, the high freezing rate would imply high nucleation rate of ice with low or no crystal growth.[8] This will result in large amount of ice crystals with small sizes, and the final graphene aerogels have small pore sizes.[10] On the other hand, at high freezing temperature of -20 °C, the ice solidification rate is low, favoring crystal growth with less nucleation. This results in fewer ice crystals and larger crystal sizes. When the ices are removed via sublimation using freezing dryer, larger crystal sizes result in networks with larger pore sizes. Therefore, since the freezing rate controls the nucleation and growth of ice crystals, the freezing temperature become the critical factor determining the morphology of the macropores in the aerogel.[8]

The mesoporous structures of the graphene networks were further verified by N_2 adsorption-desorption analysis. In Fig. 2d, all the aerogels fabricated at the different freezing temperatures showed a type IV isotherm with H3-type hysteresis loop, which indicate that mesopores have cylindrical pore geometries.[19] The aerogel made at higher freezing temperature shows higher absorbed volume, corresponding to larger specific surface area. The specific surface areas of these aerogels were calculated as 504, 441, and 315 $m^2 g^{-1}$, for the freezing temperatures -20 °C, -80 °C, -200 °C respectively by the Brunauer-Ennett-Teller (BET) method (Fig. 2d). Figure 2e shows the pore size distribution of the graphene aerogels made at the three different temperatures. The aerogel made at -20 °C shows the highest pore volume in the pore diameter range of 2 to 50 nm (mesopores). Combined with the SEM images showing larger than micrometer sized pores, we conclude that our aerogels possess hybrid structures consisted of both mesopores and macropores, with the -20 °C sample possessing the largest volume in both types of pores. As a comparison with the recent development of porous graphene structure with exceptionally high specific surface area (3523 $m^2 g^{-1}$),[10] although the specific surface area of our graphene aerogels here are 6-10 times lower, the specific capacitance (shown later) are actually higher under the same measurement conditions. This indicates that even though surface area plays an important role

in the capacitor performance, the porous structure (such as having both types of pores (mesopores and macropores)) also plays a critical role, because combination of the two types of pores ensure effective transportation of ions.[20]

We have carried out electrochemical measurements to study the performance of these porous graphene aerogels as electrodes in electrical double-layer capacitors (EDLCs). The graphene aerogels with different porosities from three freezing temperatures serve as the anode and cathode, mechanically separated by a piece of cotton paper as the separator, which are electrically connected to each other via the electrolyte. The small mesopores within the interconnected macroporous network of the aerogels are expected to provide high permeability to electrolyte ions. Cyclic voltammetry (CV) is performed to evaluate the capacitance of the graphene aerogel (-20, -80, and -200 °C) supercapacitors with all three different porosity in 0.5 M H_2SO_4 electrolyte. The CV curves of the graphene aerogel supercapacitors are measured with various scan rates in the ranges of 20 ~ 500 mV s^{-1}. All CV curves show a very rapid current response on the voltage reversal at each end potential. The rectangular shapes of these curves indicate a very small equivalent series resistance of electrodes, corresponding to fast ionic diffusion in the electrolyte. Particularly for the case of the aerogel dried at -20 °C of freezing temperature (Fig. 3a), nearly rectangular shaped CV curves are obtained even at very high scan rates, demonstrating high performance capacitor devices (for the devices from -80 and -200 °C freezing temperatures, see Fig. S3a and S3b†). Fig. 3b shows the capacitance calculated from the CV curves as a function of the freezing temperatures and scan rates. The capacitance increased as the scan rates decrease, and the graphene aerogel fabricated from -20 °C freezing temperature has the highest capacitance of 255 F g^{-1} at 20 mV s^{-1} of scan rate.

In Fig. 3c, galvanostatic charge/discharge (CD) is also conducted at different current densities to evaluate the specific capacitance and internal resistance of the graphene aerogel

supercapacitor device (for the devices from -80 and -200 °C freezing temperatures, see Fig. S3c and S3d†). The E-t responses of the charge process show a nearly triangular shape and mirror image with corresponding discharge counterparts confirming the formation of an efficient capacitor and excellent charge propagation across two electrodes. The specific capacitances calculated from discharge curves are 125, 230, 325 $F\,g^{-1}$ at 1 $A\,g^{-1}$ for graphene aerogel supercapacitors made at -200, -80, and -20 °C freezing temperatures, respectively (Fig. 3d). For the graphene aerogel supercapacitor of -20 °C freezing temperature, where electrochemically active surface and porosity is maximized, measured specific capacity is 2.6 times higher than -200 °C graphene device and 1.35−1.7 times and 1.4 times higher than 3D graphene supercapacitors in aqueous[21-22] and ionic liquid[10] electrolytes.

Fig. 3e compares energy densities calculated from the CD curves as function of discharge current density. Energy density increases with decreasing current density, and has the highest value of 45 $Wh\,kg^{-1}$ from the aerogel obtained -20 °C freezing temperature. The high freezing temperature greatly improves electrochemical performances of graphene aerogel supercapacitor due to the more effective combination of interconnected mesopores and macropores in aerogels. The mesopores are essential for high energy storage[20] and furthermore macropores in graphene aerogels can accelerate the kinetic process of ion diffusion. Therefore, our methods to tailor pore sizes in macropore regime with mesopore sizes suggest effective direction for high performance supercapacitors.

To evaluate energy storage performance of graphene aerogel devices, energy densities are plotted versus power density (Ragone plot) as shown in Fig. 3f. The gravimetric energy density of the graphene aerogel-based supercapacitor fabricated at -20 °C shows higher value than the graphene aerogel devices of -80 and -200 °C freezing temperatures. This remarkable capacitor behavior can be attributed to the well-controlled pore size features on the electrode, the increased surface area, and the maximized active electrochemical surface area and hybrid

porosity. The Ragone plots are also compared with carbon-based supercapacitors performed in H_2SO_4 electrolyte.[23-29] The maximum energy density of the graphene aerogel-based supercapacitor is 45 Wh kg^{-1}. This value is significantly higher than that of other supercapacitors. The power density of graphene aerogel devices is still higher than that of the most of other supercapacitors. Although some shows larger power density than ours, those were performed in 10 times higher concentration H_2SO_4 electrolyte of 5 M (S2)[24], or at high measurement temperature of 60 °C (S3)[25] causing irreversible redox reactions or by using metal oxide (RuO_2) assistants and polyaniline pseudocapacitor (S4).[26] As far as we know, the combination of the energy density and power density of the graphene aerogel electrodes shows excellent performance, and is among the best reported values for EDLCs using aqueous electrolyte.

In general, the total energy that can be stored in a single supercapacitor is not enough for many applications. To further demonstrate the practical usage and the reliability of the high performance supercapacitors based on graphene aerogels, we connected three supercapacitor units in series to create a tandem device. Each supercapacitor unit has the same mass loading of graphene aerogels fabricated at -20 °C freezing temperature. Cyclic voltammetry in Fig. 4a performed at a scan rate of 50 mV s^{-1} and its potential window extends to 4.0 V for such tandem device. A voltage scan in the range from 0.8 to 3.6 V did not reveal any significant increase of anodic current, even if a small increase of the measured current can be observed during the scanning. It means that the electrolyte is not being decomposed, where the minimum decomposition voltage of water at 25°C is about 1.25 V. The practical voltage of over 3V can be successfully applied for a capacitor operating in this electrolyte. The adaptability of graphene aerogel supercapacitors for galvanostatic charge/discharge cycling is demonstrated by connecting three devices together both in series and in parallel configurations (Fig. 4b-c). Galvanostatic cycling was performed at current density of 1 A g^{-1}

and 2 A g^{-1} for series and parallel connections, respectively. Similar to the individual units, the tandem devices exhibit nearly ideal triangular charge/discharge curves which indicate excellent capacitive properties. Especially, in series connection, the device shows practically unchanged charge/discharge time, suggesting the performance of each supercapacitor unit is well retained in series and parallel connections.

Electrochemical impedance spectroscopy in the frequency range from 10 mHz to 100 kHz was performed to confirm the superior performance of the graphene aerogel supercapacitor. From the curve shape of the impedance measurement, pore geometry can be derived, and the result of V-shaped pore geometries were observed from all the device units.[30] Such a shape would imply that small ions can permeate through all electrode surface without obstruction and constrain, which explains the reason for the high performance of these aerogel electrodes. The equivalent series resistance obtained at the highest frequency (100 kHz) on the real axis is only 3.6 Ω for one supercapacitor unit and 10.7 Ω for three units, which directly proves that the charges transfer at the electrode/electrolyte interface is very quick and current can pass very easily through the interface with low internal resistance. Finally we measured the long cycle life (number of charge-discharge cycles at constant current) of three tandem supercapacitors. The normalized capacitance and the coulombic efficiency as a function of cycle-number are shown in the Fig. 5. The supercapacitor devices show long life cycle stability: > 98% coulombic efficiency of the initial capacitance after 5,000 cycles, allowing practical applications for high power and high voltage operation.

In conclusions, we demonstrated the design of graphene aerogel supercapacitors with high performance from the electrochemically exfoliated larger-area thin graphene sheet suspensions. Compared with other methods to achieve graphene solutions, the electrochemical exfoliation has high throughput and scalability, and the produced graphene

sheets have high aspect ratio and quality. These characteristics facilitate the production bulk porous graphene structures at large scale with low cost. We have also found that the aspect ratios of the graphene flakes can be optimized by tuning the conditions during the electrochemical exfoliation. This allows the optimization of the structures in the graphene aerogel to achieve the best performances in their applications. Furthermore, the porous structure of graphene aerogels can also be tuned by the freezing temperature in the freeze drying process. The unique morphological and structural features of the graphene aerogels maximize the active electrochemical surface area and porosity, leading to high energy storage performance. Especially, interconnected meso- and macropores of graphene aerogels can provide fast ion channels to facilitate ion transport for high performance. The graphene electrodes obtained from this method demonstrate excellent uniformity and stability, which allows the construction of cells in parallel and series, enabling the high voltage operation even with aqueous electrolyte. Combining with the efficient and low cost production of graphene solutions from the electrochemical exfoliation, our work here demonstrate a feasible route for graphite powder in practical energy storage applications.

Experimental Section

Fabrication of graphene suspensions: The graphene suspension with high-quality thin graphene sheets was obtained by electrochemical exfoliation of natural graphite flakes.[17] For the electrochemical exfoliation, two graphite electrodes were immersed into the electrolyte solution as an anode and cathode. In order to minimize graphene oxidation by the acidic electrolyte (0.2 M sulfuric acid (H_2SO_4)), different concentrations (23, 30, and 37 w%) of potassium hydroxide (KOH) was added to obtain the optimized result with largest aspect ratio (lateral dimension: thickness) of the graphene sheets, and uniform dispersion of graphene without surfactant at high concentration. The electrochemical exfoliation process was carried

out by applying alternating current (±1 A) with a duration time of 5 seconds for each. As a result, the graphene sheets were exfoliated alternatively from one graphite electrode at 10-15V. The exfoliated graphene sheets were collected with a 100 nm porous filter and washed with DI water by filtration. Then, the exfoliated graphene sheets were very uniformly dispersed in ethanol.

Fabrication of graphene aerogels: The aerogel fabrication is based on our previous study[16] via the assembly of anisotropic nano-objects into a cross-linking network from their colloidal suspensions at the transition from the semi-dilute to the isotropic concentrated regime. The thickness and sheet size of the exfoliated graphene optimized to fabricate the graphene aerogel were about 2.5 nm and 3.7 μm at the 30 wt% KOH in H_2SO_4 aqueous solution. The dilute suspensions of the exfoliated graphene were evaporated slowly at 313 K to transform them into more concentrated suspensions (gels) with a large volume compression. As the concentration increase, some graphene sheets are physically contacted with each other through van-der Waals forces and at higher concentration, a 3D network is formed by these interconnected branches composing of graphene sheets and thus a graphene gel is obtained. After that, ethanol in the pore of the gel was exchanged into DI water, which is then removed via freeze-drying technique. For the freeze drying process, the graphene gels were first frozen at different temperatures (-200 °C, -80 °C, and -20 °C). The ice is removed by sublimation using freezing dryer to ensure the porous network without shrinking or collapsing.

Property characterizations: Atomic force microscope (AFM, Dimension 3100, Veeco system) measurements were carried out to characterize the thickness and size of the graphene sheets. Scanning electron microscopy (JEOL 6700F) was used to characterize the porosities of the aerogel networks. Nitrogen adsorption and desorption isotherms for the porosities of the aerogels were measured at 77 K on a Micromeritics ASAP 2010 system. Before the measurement, the samples were degassed at 423 K under vacuum ($<10^{-4}$ mbar) for several hours. Surface areas of the aerogels were calculated from the Brunauer-Ennett-Teller (BET)

method with multi-molecular layer adsorption model. The electrical conductivities of the graphene aerogel at room temperature were measured using a four-probe station for porous materials. The resulting errors in the electrical conductivity measurement are estimated to be less than 5 %.

Characterizations of supercapacitor devices: The graphene aerogels were used directly as anodes and cathodes for assembling symmetric supercapacitors in 0.5 M H_2SO_4 aqueous electrolyte. Electrochemical properties of graphene aerogel-based supercapacitors are analyzed using cyclic voltammetry (CV), galvanostatic charge-discharge (CD), electrochemical impedance spectroscopy (EIS) and cyclic stability by Potentiostat (VersaSTAT 4) at room temperature. The CV curves are measured between 0 and 1 V for one unit supercapacitor in 0.5 M H_2SO_4 electrolyte with various scan rates in the range of 10–500 mV s^{-1} and between 0 and 4V for three tandem supercapacitors. To quantitatively evaluate the charge storage capacity at each scan rate, the capacitance of the graphene aerogel is calculated based on the following method[31]: $C=\int_{E_1}^{E_2} i(E)dE/2(E_2-E_1)mv$, where C is the capacitance of the sample, E_1, E_2 are the cutoff potentials in the cyclic voltammetry, $i(E)$ is the instantaneous current, $\int_{E_1}^{E_2} i(E)dE$ is the total voltammetric charge obtained by integration of positive and negative sweep in cyclic voltammograms, (E_2-E_1) is the potential window width, and m is the mass of a single electrode. The CD curves are obtained at a constant current density in the range of 1 to 20 A g^{-1}. The capacitance and internal resistance values are determined from the slope and the initial voltage drop of the galvanostatic CD curves, respectively. The specific capacitances, C_s are calculated from the galvanostatic discharge curves[32] using $C_s = i/-[\Delta V/\Delta t]m = i/-\text{slope} \times m$, where i is the discharge current, and the slope is the slope of the discharge curve after the iR drop. For the EIS, the amplitude of the AC signal applied to the electrodes was 50 mV and the frequency was varied from 10 mHz to 100 kHz. The efficiency (η), the power density (P) and energy density (E) are calculated using $\eta=(t_d/t_c)\times100$,

$P=V^2/[4Rm]$ and $E=0.5CV^2/m$, respectively where t_d is the discharging time, t_c is the charging time, and R is the internal resistance, respectively.

Acknowledgements

The authors gratefully acknowledge the support through the STC Center for Integrated Quantum Materials from NSF grant DMR-1231319. S. M. J acknowledges MIT Institute of Soldier Nanotechnologies (ISN) for the access of various instruments to carry out this work. D. L. M. acknowledges the Brazilian agency CNPq.

References

1. A. Peigney, C. Laurent, E. Flahaut, R. R. Bacsa and A. Rousset, *Carbon,* 2001, **39**, 507.

2. S. Han, D. Wu, S. Li. F. Zhang and X. Feng, *Adv. Mater.* 2014, **26**, 849.

3. A. K. Geim and K. S. Novoselov, *Nature Materials,* 2007, **6**, 183.

4. Z. Chen, W. Ren, L. Gao, B. Liu, S. Pei and H-M. Cheng, *Nature Materials,* 2011, **10**, 424.

5. J. Hu, Z. Kang, F. Li and X. Huang, *Carbon,* 2014, **67**, 221.

6. F. Zeng, Y. Kuang, G. Liu, R. Liu, Z. Huang, C. Fu and H. Zhou, *Nanoscale,* 2012, **4**, 3997.

7. D. Brownson, D. K. Kampouris and C. E. Banks, *J. Power Source,* 2011, **196**, 4873.

8. X. Xie, Y. Zhou, H. Bi, K. Yin, S. Wan and L. Sun, *Sci. Rep*., 2013, **3**, 2117.

9. C. Li and G. Shi, *Nanoscale,* 2012, **4**, 5549.

10. L. Zhang, F. Zhang, X. Yang, G. Long, Y. Wu, T. Zhang, K. Leng, Y. Huang, Y. Ma, A. Yu and Y. Chen, *Sci. Rep*., 2013, **3**, 1408.

11. M. A. Worsley, P. J. Pauzauskie, T. Y. Olson, J. Biener, J. H. Satcher and T. F. Baumann, *J. Am. Chem. Soc*., 2010, **132**, 14067.

12. G-N. Cristina, R. T. Weitz, A. M. Bittner, M. Scolari, A. Mews, M. Burghard and K. Kern, *Nano Lett*. 2007, **7**, 3499.

13. J. Zou, and F. Kim, *Nat. Commun*., 2012, **3**, 1241.

14. L. Qiu, J. Z. Liu, S. L.Y. Chang, Y. Wu, and D. Li, *Nat. Commun*., 2014, **5**, 5254.

15. W. Ouyang, J.Sun, J. Memon, C. Wang, J. Geng, and Y. Huang, *Carbon*, 2013, **62**, 501.

16. S. M. Jung, H. Y. Jung, M. S. Dresselhaus Y. J. Jung and J. Kong, *Sci. Rep*., 2012, **2**, 849.

17. C. Y. Su, A. Y. Lu, Y. P. Xu, F. R. Chen, A. N. Khlobystov and L. J. Li, *ACS Nano,* 2011, **5**, 2332.

18. K. Parvez, Z-S. Wu, R. Li, X. Liu, R. Graf, X. Feng and K. Müllen, *J. Am. Chem. Soc*., 2014, **136,** 6083.

19. S. J. Gregg and K. S. W. Sing, Adsorption, Surface Area and Porosity, Academic Press, New York, 1982.

20. T. Y. Kim, G. Jung, S. Yoo, K. S. Suh and R. S. Ruoff, *ACS Nano,* 2013, **7**, 6899.

21. Y. Xu, Z. Lin, X. Huang, Y. Wang, Y. Huang and X. Duan, *Adv Mater.,* 2013, **25**, 5779.

22. Y. Xu, K. Sheng, C. Li and G. Shi, *ACS Nano,* 2010*,* **4***,* 4324.

23. W. Wang, Q. Hao, W. Lei, X. Xia and X. Wang, *RSC Advances,* 2012, **2**,10268.

24. H. Zhang, V. V. Bhat, N. C. Gallego and C. I. Contescu, *ACS Appl. Mater. Interfaces.,* 2012, **4**, 3239.

25. Z. Xu, Z. Li, C. Holt, X. Tan, H. Wang, B. S. Amirkhiz, T. Stephenson and D. Mitlin, *J. Phys. Chem. Lett.,* 2012, **3**, 2928.

26. J. Zhang, J. Jiang, H. Li and X. S. Zhao, *Energy Environ. Sci*., 2011, **4**, 4009.

27. D. Puthusseri, V. Aravindan, S. Madhavi and S. Ogale, *Energy Environ. Sci*., 2014, **7**, 728.

28. Y. Xu, Z. Liu, X. Huang, Y. Liu, Y. Huang and X. Duan, *ACS Nano,* 2013, **7**, 4042.

29. L. T. Le, M. H. Ervin, H. Qiu, B. E. Fuchs and W. Y. Lee, *Electrochem. Commun*., 2011, **13**, 355.

30. H. Keiser, K. D. Beccu and M. A. Gutjahr, *Electrochim. Acta,* 1976, **21**, 539.

31. W. Chen, Z. Fan, L. Gu, X. Bao and C. Wang, *Chem. Comm*., 2010, **46**, 3905.

32. H. Y. Jung, M. B. Karimi, M. G. Hahm, P. M. Ajayan and Y. J. Jung, *Sci. Rep*., 2012, **2**, 773.

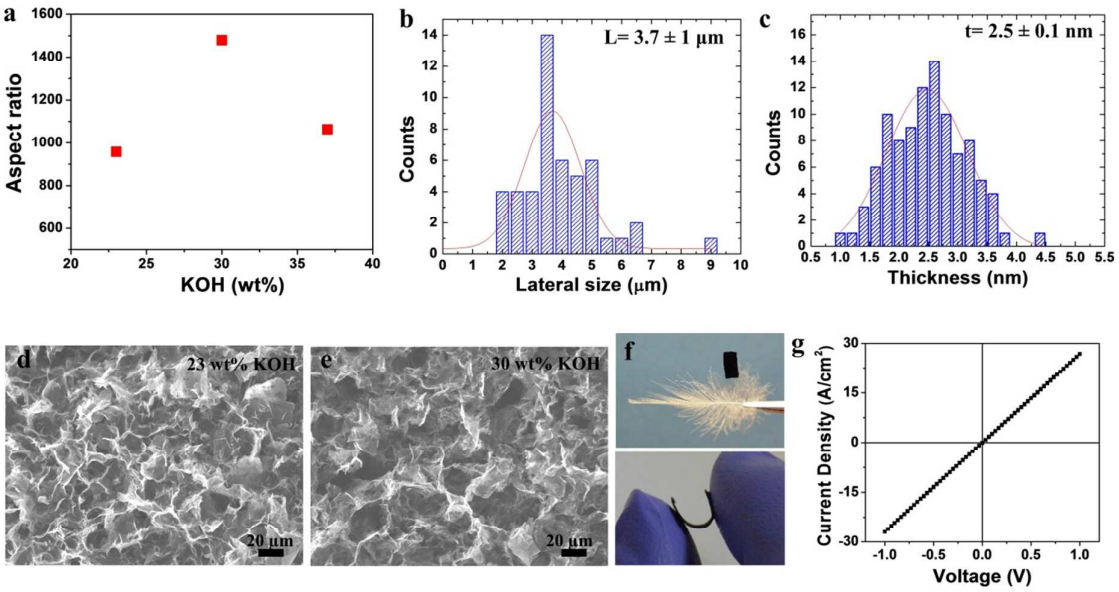

Fig. 1 (a) The aspect ratio of the exfoliated graphene sheets at 23, 30, and 37 wt% KOH in H_2SO_4 electrolyte. The sheet size (b) and thickness (c) distribution of exfoliated graphene for 30 wt% KOH in H_2SO_4 electrolyte. The average sheet size is about 3.7±1 µm and the average thickness is 2.5±0.1 nm. (d,e) SEM images of aerogels using graphene sheets exfoliated at 23 (d) and 30 (e) wt% KOH in H_2SO_4 electrolyte (-20 °C freezing temperature was used for the freeze drying step). (f) Optical pictures showing ultralight, flexible and bendable natures of as-prepared graphene aerogels (in Fig. 1e). (g) I-V curve of the graphene aerogel in (e): electrical conductivity, $\sigma = 509\ S\ m^{-1}$.

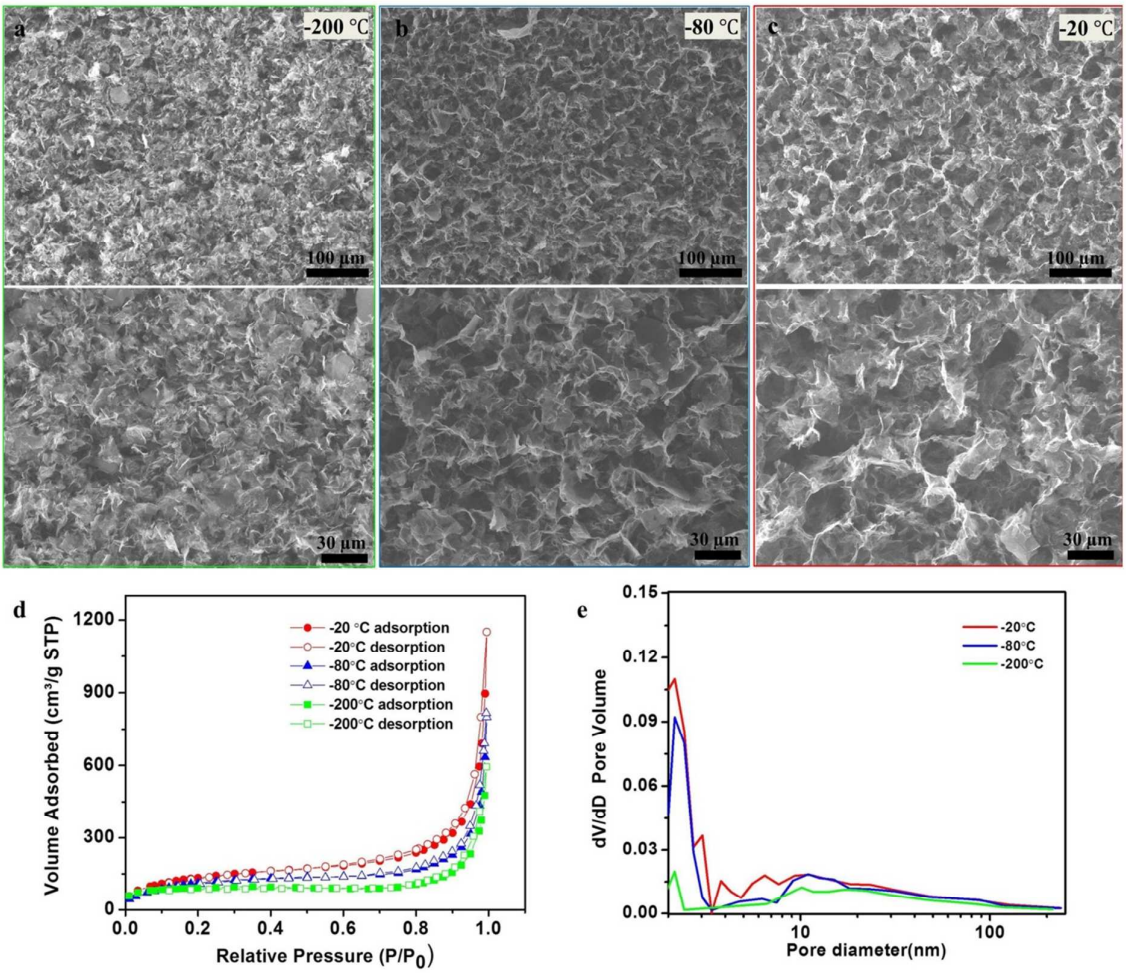

Fig. 2 SEM images of the graphene aerogels fabricated at freezing temperatures of -200 (a), -80 (b), and -20 °C (c). (d) N_2 adsorption-desorption isotherms of the freeze-dried graphene aerogels at -20, -80, and -200 °C, with 504, 441, and 315 $m^2 g^{-1}$ of specific surface areas calculated respectively by the Brunauer-Ennett-Teller (BET) method, and (e) pore size distribution of graphene aerogel made at different freezing temperatures.

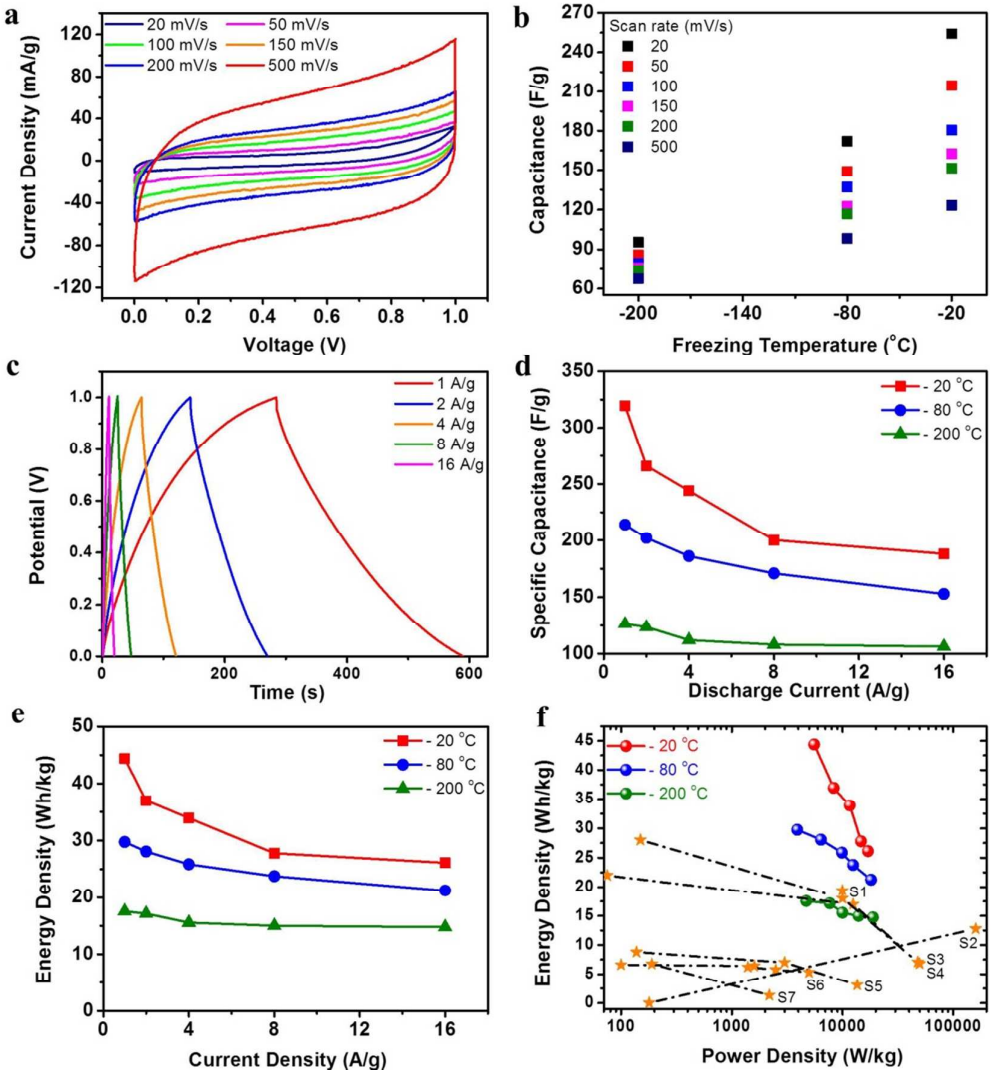

Fig. 3 (a) The CV curves of the graphene aerogel (freezing temperature of -20 °C) supercapacitors measured at various scan rates between 20 – 500 mV s^{-1}. (b) The capacitance calculated from CV curves as a function of freezing temperatures and scan rates. (c) Galvanostatic charge/discharge curves of the graphene aerogel (freezing temperature of -20 °C) supercapacitors measured at different current densities. (d) Specific capacitances of samples made at different freezing temperatures calculated from CD curves as function of the discharge current. (e) Energy densities calculated from the CD curves as a function of discharge current density. (f) Ragone plot of the graphene aerogel samples in this work compared to previous works (S1 to S7[23-29]).

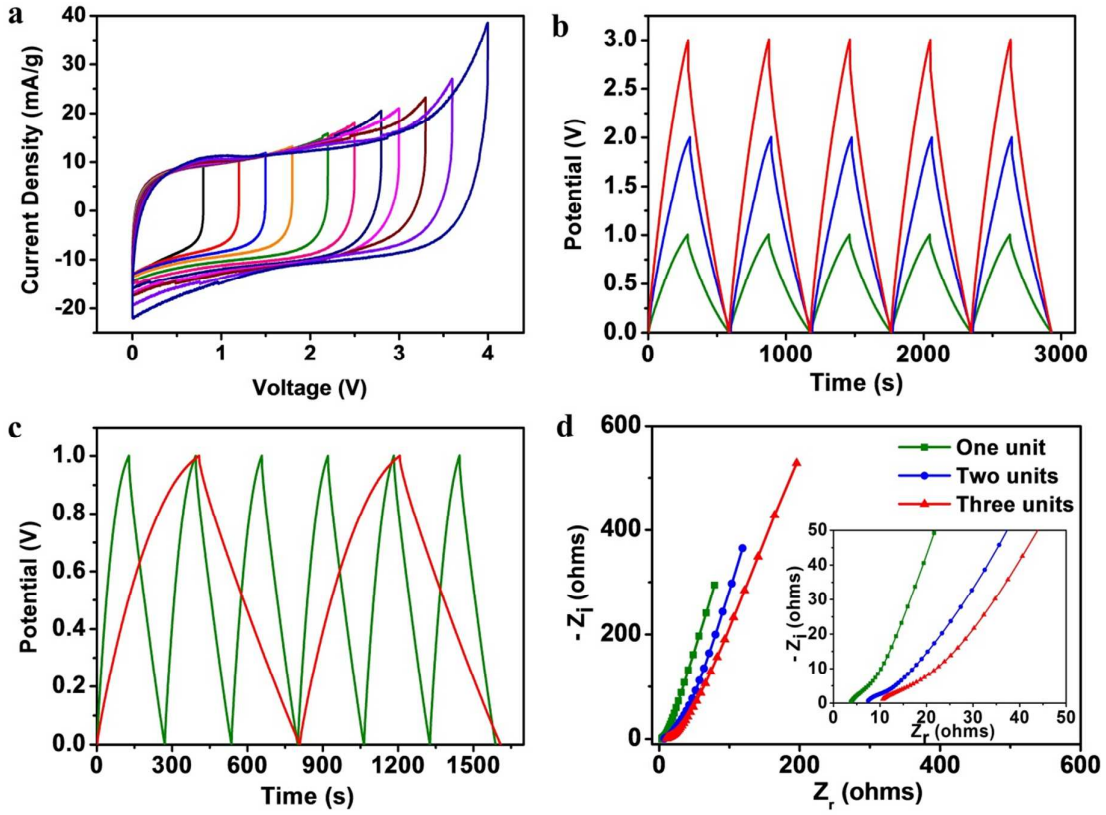

Fig. 4 (a) CV curves of a unit with three supercapacitors in series at a scan rate of 50 mV s^{-1}. Here the same colors represent single cycle scanned to a particular voltage range (0.8, 1.2, 1.5, 1.8, 2.2, 2.5, 2.8, 3.0, 3.3, 3.6, 4.0 V, respectively). b-c) Galvanostatic charge/discharge curves of supercapacitors in series (b) and in parallel (c) connection. The current density is 1 A g^{-1} for series connection ((b), green, blue and red solid line are one, two and three unit cells, respectively) and 2 A g^{-1} for parallel connection ((c), green and red are one and three parallel cells respectively). (d) Electrochemical impedance spectroscopy of a graphene aerogle electrode in the frequency range from 10 mHz to 100 kHz.

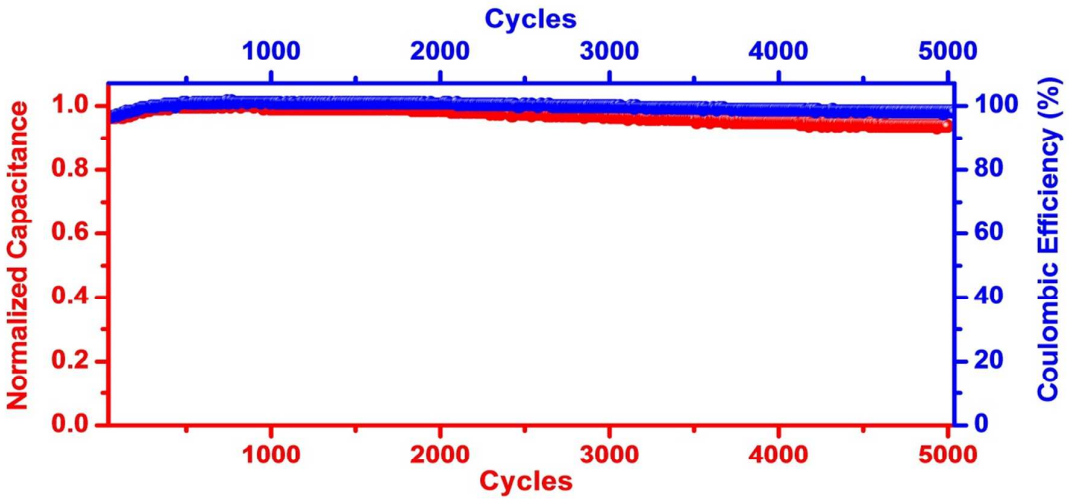

Fig. 5 The normalized capacitance and coulombic efficiency of a unit with three tandem supercapacitors during 5000 cycles.